EUROPEAN COMMISSION

Community research

BELBaR

(Contract Number: 295487)

DELIVERABLE (D-N°: D2.5)

Progress report on erosion processes under flowing water conditions

Author(s):

E. Hansen, M. Hedström, Clay Technology AB

T. Schatz, B+ Tech Oy

R. Červinka, J. Gondolli, ÚJV Řež, a. s.

F. Friedrich, F. Rinderknecht, KIT-CN/INE

Reporting period: **01/03/12 – 29/02/16**

Date of issue of this report: **05/06/14**

Start date of project: **01/03/12** Duration: 48 Months

Project co-funded by the European Commission under the Seventh Euratom Framework Programme for Nuclear Research &Training Activities (2007-2011)		
Dissemination Level		
PU	Public	PU
RE	Restricted to a group specified by the partners of the BELBaR project	
CO	Confidential, only for partners of the BELBaR project	

EURATOM

DISTRIBUTION LIST

Name	Number of copies	Comments
Christophe Davies (EC) BELBaR participants		

BELBaR Deliverable D2.5

This report contains contributions from four different research laboratories and partners in the BELBaR project, Clay Technology AB, B+ Tech Oy, ÚJV Řež, a.s. and KIT-CN/INE. It may still be premature to give general or integrated conclusions for the work that have been performed at the different laboratories. Therefore, each contribution is presented as delivered and the authors from the different laboratories draw conclusions regarding their own work. However, readers of this report may notice both similarities and differences in the way the different groups have approached the problem of studying erosion processes in bentonite/montmorillonite under flowing water conditions.

Results from Clay Technology AB

Materials and methods

Material

The erosion studies reported here have been performed using Wyoming-type (Wy) montmorillonite extracted from MX-80 bentonite (American Colloid Co.). The montmorillonite was purified and ion-exchanged with NaCl to the homoionic form according to the procedure described in (Karnland *et al*. 2006). The purified montmorillonite is referred to as Wy-Na, where Na is the counter ion. The chemical formula for an ideal sodium montmorillonite, interlayer water excluded, can be written as $[(Si_{8-\alpha}Al_{\alpha})(Al_{4-\beta}Mg_{\beta})O_{20}(OH)_4]^{(\alpha+\beta)-}Na^{+}_{\alpha+\beta}$, where by definition the tetrahedral charge is lower than the octahedral charge ($\alpha<\beta$) and the sum of tetrahedral and octahedral charges fulfil $0.4<\alpha+\beta<1.2$ (Karnland *et al.* 2006). There are two major reasons for working with Wy-Na: First, Na-montmorillonite show essentially unlimited swelling below the critical coagulation concentration (CCC), i.e. it turns into a sol, which is the reason for studying the erosion process under dilute conditions in the first place. Second, Wy-Na has the highest CCC (~20 mM NaCl) of all the clays investigated in Deliverable D4.7. Thus the erosion rates obtained using Wy-Na are pessimistic estimates, compared to the possible future conditions in a High-Level Waste (HLW) repository.

Equipment

The artificial fractures, made of poly(methyl methacrylate), were square with an inside width of 21 cm. In the set of experiments reported here, two apertures, 120 μm and 240 μm have been used. The artificial fracture is equipped with an inlet and outlet, allowing us to flow various solutions through the cell (Figure 1). Similar equipment has been used by Schatz et al (2013), but there are some differences, e.g. in our fracture system the clay can only take up water from the slit whereas in the B+ Tech equipment the clay may also be in contact with water through filters on top and bottom of the clay puck.

The artificial fractures used for erosion measurements were equipped with an additional in- and outlet at the outlet side thereby allowing for flushing the outlet slit collecting eroded material that may gather there. At the centre of the fracture system there is room for a clay puck of diameter 35 mm and thickness ~10 mm.

The amount of eroded montmorillonite was measured using a portable turbidimeter TN-100 from Eutech Instruments. The light source in the turbidimeter is an infrared-emitting (850 nm) diode. The intensity of the scattered light is directly converted to nephelometric turbidity units (NTU) by the instrument. At low clay concentrations (<5 g/L), the turbidity response have been found to be linear. The mass of eroded clay particles can thus be calculated through the

equation $m_{clay}=(N \cdot V)/114$ where m_{clay} is the mass of the eroded clay (g), *N* is the turbidity (NTU) and V is the volume of the suspension (L) (Birgersson *et al*. 2009).

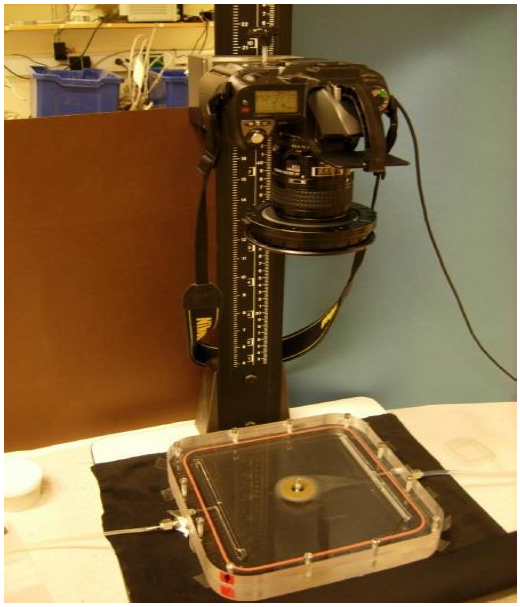

Figure 1. *Experimental set-up.*

Method

The montmorillonite was dried *in vacuo* overnight, followed by saturation with deionized water in a test cell similar to the ones used by ClayTech for measuring swelling pressures (Karnland et al., 2006). The initial dry density of the montmorillonite is 1257 kg/m^3 which gives a water-saturated density of 1800 kg/m^3. The water-saturated clay puck was transferred to the artificial fracture, with care taken not to allow the clay to dry. The fracture was closed and filled with degassed deionized (DI) water.

During free swelling experiments, the artificial fracture was filled with degassed DI water, after which the clay was allowed to swell into the fracture. This was photographically documented, with pictures taken at suitable intervals depending on the rate of expansion.

During erosion measurement experiments, aqueous solution, also prepared from degassed DI water, was flowed through the artificial fracture. The start- and end times of the erosion measurement were recorded. When the flow was stopped, the collected suspension was weighted. The outlet slit was flushed with degassed DI water to collect eroded material which had gathered in the outlet slit, and the flushed-through suspension was also weighted. Turbidity measurements were used to determine the amount of eroded colloidal clay particles in both water volumes.

Results and discussion

Free swelling – deionized water

The free swelling behaviour was investigated at two different fracture apertures, 120 μm and 240 μm, in DI water. Initially, the swelling into the fracture progressed rapidly at both 120 μm and 240 μm. While the swelling progressively slows down, during the experimental time scale it does not cease completely. At 120 μm, closest to the clay puck we find a repulsive paste, quite well-defined and thick enough to appear very bright in colour (scattered light from the camera flashes) (Figure 2a). This paste is strong enough that as it expands, it pushes air

bubbles in the fracture ahead of itself, rather than surrounding them. Further out, there is a sol of varying (and not yet determined) clay concentration. At the interface between the sol and the DI water a fingering instability occur, akin to the Rayleigh-Taylor instability (RTI) that occurs when a denser liquid is placed on top of a less dense liquid and is pulled down by gravity. The RTI fingers are particularly well resolved in the thinner fracture Figure 2a. In this case it is not gravity that is the driving force for the RTI but water transport into the clay.

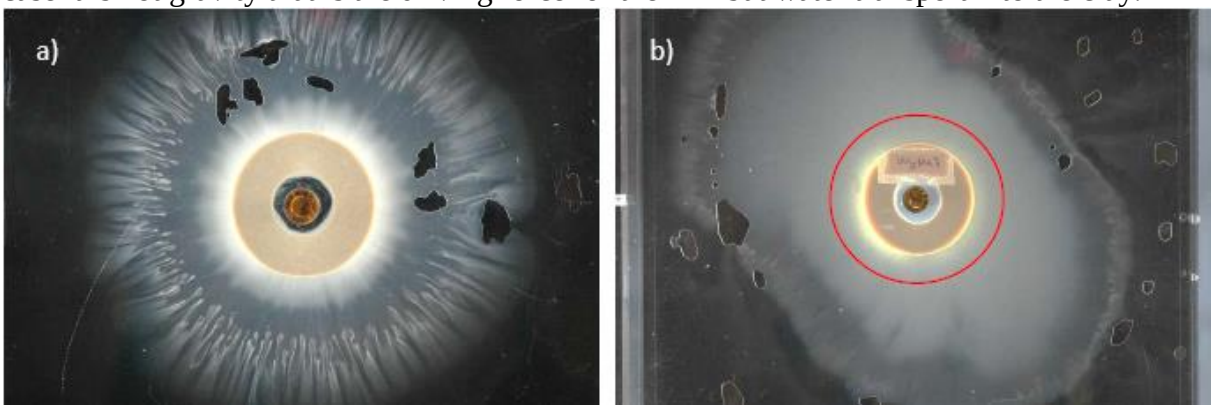

Figure 2. *Free swelling in deionized water after 30 days at a) 120 µm aperture and b) 240 µm aperture. The red circle in b) shows the extent of extrusion (swelling) of paste (the brighter area outside the montmorillonite puck in a) into the fracture at 120 µm for comparison. When there is a flow through the cell, all clay outside the brighter paste, is transported away.*

The same phases, the thick paste and the sol, are found during free swelling at an aperture of 240 µm (Figure 2b). Also RTI can be found, although the fingers are less well-resolved at the broader aperture. As in the case of 120 µm aperture, the paste is sufficiently thick to push air bubbles ahead during swelling rather than encompassing them. For comparison, the edge of the corresponding paste is outlined in Figure 2b, which gives an idea of the difference in swelling capability at different apertures.
The paste, the thicker clay phase closest to the puck, is found not to mechanically erode under our conditions, even at the highest flow rates. However, as swelling is a continuous process, particles that disperse from the paste to form a sol are easily flowed away into the fracture.

Free swelling – 25 mM NaCl-solution
The free swelling behaviour in a solution with higher salinity was also investigated. When setting up this experiment, clay was mechanically extruded into the fracture when the fracture was closed, thus the clay in the fracture has the same density as in the puck. This point constitutes the starting point for swelling, and has been outlined with a red circle in Figure 3. During the initial 48 h, some swelling (1-2 mm) is evident. Despite this, after the initial two days no more swelling is experienced and the clay appears to have formed a stable gel at the edges, which does not release sol particles into the fracture. Even with a flow of 25 mM NaCl-solution, there are no signs of erosion. In fact, decreasing the salinity to 20, 15 or 10 mM NaCl still causes no erosion during flow. In order to see any sign of erosion, the salinity of the solution had to be decreased to 5 mM NaCl. This suggests the presence of some sort of hysteresis, which might affect the montmorillonite loss in the actual HLW repository.

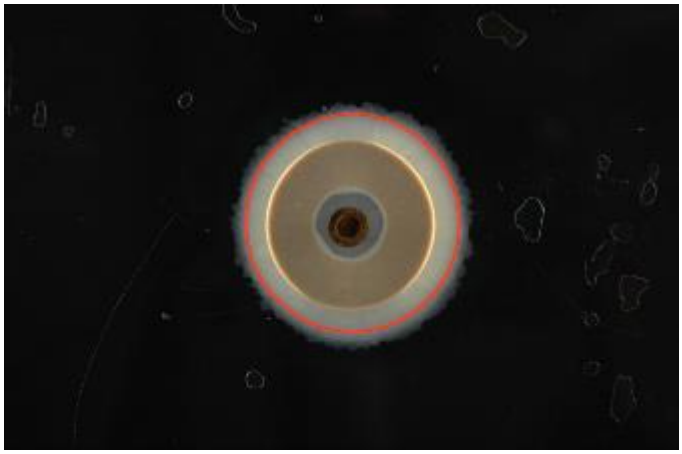

Figure 3. *Free swelling in 25 mM NaCl-solution at an aperture of 120 µm. The saturated density of the montmorillonite is 1800 kg/m*^{3}

Erosion measurement

Initial erosion measurements were performed at a fracture aperture of 120 µm (Figure 4). The measurements commenced at 5 mM NaCl (aq). As expected, since CCC is ~20 mM, the erosion was found to increase with increasing flow rate. By raising the salinity to 10 mM NaCl (aq), the erosion was decreased. However, it was still increasing with flow rate. After increasing the salinity to 15 mM NaCl (aq), the erosion during the first 48 h was roughly half the erosion at the corresponding flow rates at 10 mM NaCl. Within a week, erosion had completely ceased or was below the detection limit. The salinity was further increased to 20 mM NaCl, as 20 mM NaCl has been reported as the CCC value of Wyoming montmorillonite clay (Birgersson *et al*. 2009). As expected, there were no signs of erosion.

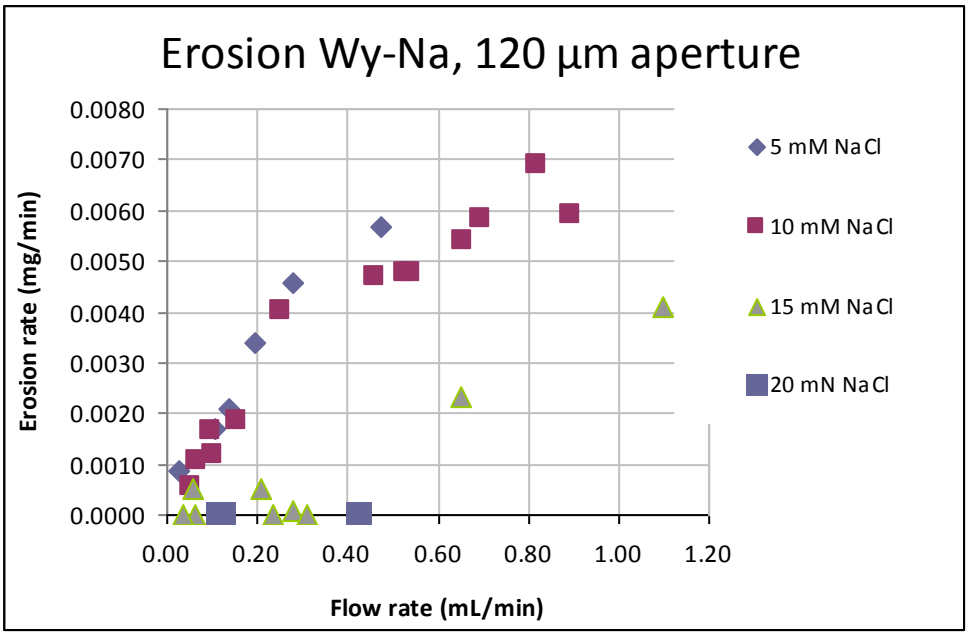

Figure 4. *Erosion of Wy-Na in an artificial fracture with aperture 120 µm. Salinity was increased from 5 mM NaCl to 20 mM NaCl.*

After the salinity had been increased from 5 mM NaCl to 20 mM NaCl, we decided to test if erosion would commence at 10 mM NaCl as previously erosion ceased upon increasing the salinity from 10 mM NaCl to 15 mM NaCl. The salinity of the aqueous solution was first decreased to 15 mM NaCl before erosion measurements at 10 mM NaCl was started. Despite the fact that the erosion measurements were performed during a month's time, which should have been ample time for the clay to reach a new Donnan equilibrium with the new solution (Birgersson and Karnland 2009; Karnland and Hedström, 2012), there were no signs of erosion during any of the measurements. Therefore, the salinity was decreased to 5 mM NaCl. Yet again, there were no signs of erosion during the initial measurements. However, after 16 days, erosion commenced. The erosion measurements were continued during two months, in order to investigate whether erosion during this time period reaches the erosion at the initial 5 mM NaCl-measurements. Despite this, the erosion did not appear to approach the earlier erosion levels (Figure 5). It is of course possible that given enough time, the erosion will be similar whether the NaCl-concentration is increased from deionized water, or decreased from a higher NaCl-concentration, but it is not obvious on this time scale. Consequently, there appear to be a considerable hysteresis effect, where the history of the clay sample appears to play a significant role in the erosion of montmorillonite clay. This illuminates the difficulty in reaching conclusions as to the CCC, the phase behaviour or the erosion susceptibility of montmorillonite.

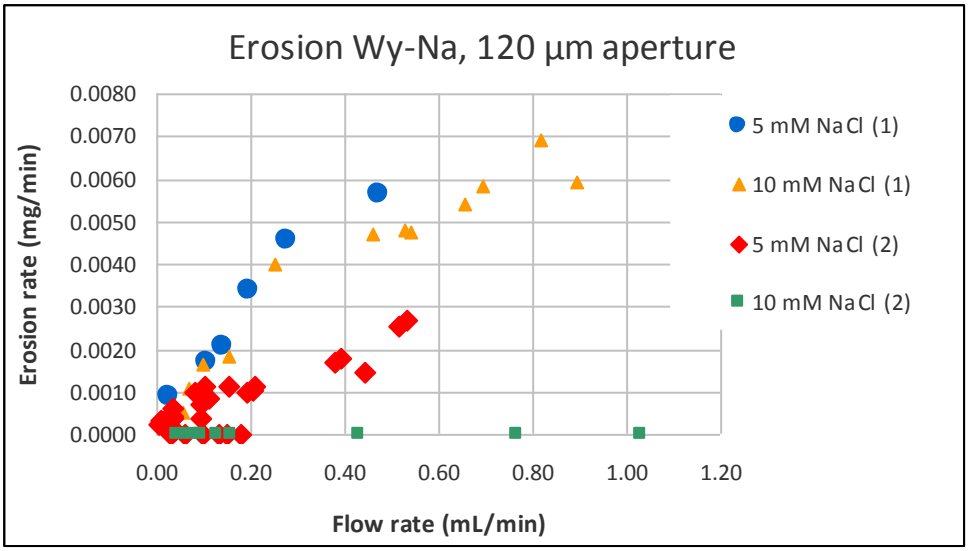

Figure 5. *Erosion rates v.s flow rate for the case where first the NaCl concentration in the flowing solution was increasing (1). After reaching 20 mM NaCl the concentration in the flowing solution was decreased (2).*

Erosion measurements at an aperture of 240 µm commenced with deionized water. When shifting to 5 mM NaCl-solution, the erosion difference at low flows was marginal, although the difference in erosion at higher flows was more significant (Figure 6).

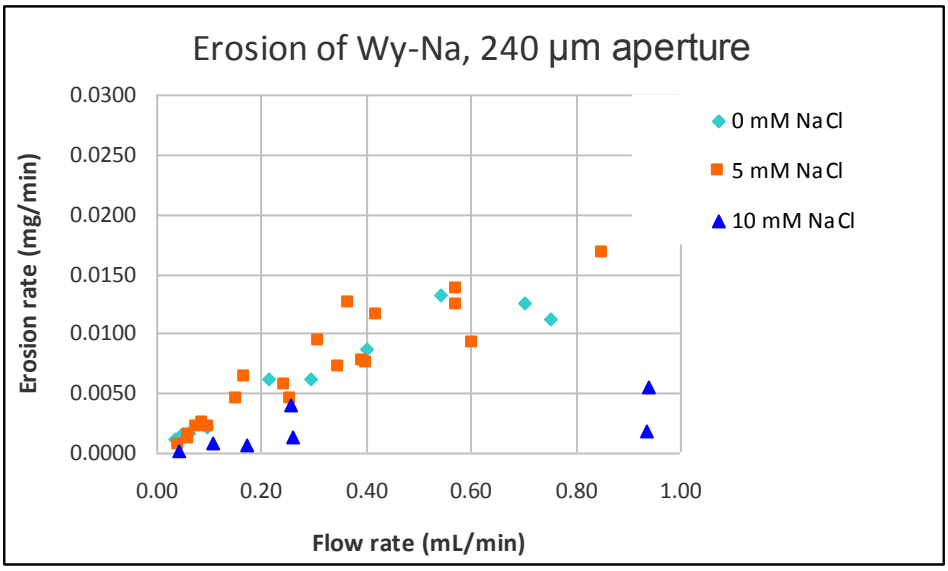

Figure 6. *Erosion of Wy-Na in an artificial fracture with aperture 240 µm. Salinity was increased from 0 mM NaCl to 10 mM NaCl.*

Comparison of erosion at different fracture apertures

When we compare the erosion at different fracture apertures, we find that the erosion, in addition to the salinity of the system, also depends on the fracture aperture. One has to take into account that in Figure 7 the erosion rate is plotted against flow rate given as volume per time, thus at the same flow rate the flow velocity at the larger aperture is lower. Without any clay present the velocity would be precisely a factor two lower in the 240 µm fracture compared to the 120 µm fracture at the same flow rate. Due to larger extrusion of clay in the wider fracture the difference in flow rate must be less than a factor two. The results in Figure 7 show that at 5 mM, erosion rate is larger in the wider fracture also taking velocity into account. However at 10 mM NaCl the erosion rates vs. flow velocity are more or less the same for the two apertures.

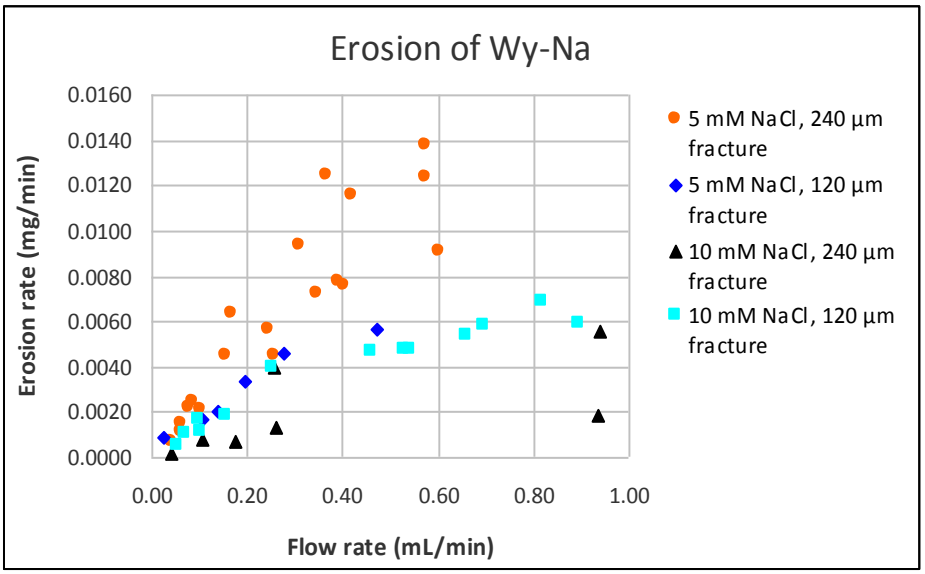

Figure 7. *Comparison of erosion rates of Wy-Na in artificial fractures with apertures 120 µm and 240 µm. Salinity was increased from 0 mM NaCl to 10 mM NaCl.*

Conclusions

We have confirmed the connection between the flow rate and the erosion, when the NaCl concentration is well below the CCC. As the salinity increases, erosion decreases. At an aperture of 120 μm, the erosion eventually ceases when the salinity in the system is 15 mM NaCl. For the aperture of 240 μm the test has not yet been performed above 10 mM but the tests at 10 mM NaCl indicate a clear reduction in erosion rate. In fact the erosion rates vs. flow velocity are the same for 120 and 240 μm apertures at 10 mM NaCl, possibly indicating the formation of stable structures at that salinity. However, more data are needed to verify this and to rule out other explanations.

Furthermore, we see a hysteresis effect present, that is, the history of the clay will affect the erosion capability of the clay. That means that a montmorillonite clay that erodes at a salinity of 10 mM NaCl, might be completely stable against erosion, if it has previously had a higher salinity present, during which the clay particles at the clay-solution interface could form a gel. This suggests that not only is control of the boundary conditions of importance for evaluating erosion rates; awareness of the system's history seems also crucial.

References

Birgersson M., Börgesson L., Hedström M., Karnland O., Nilsson U. (2009). Bentonite erosion – Final report. SKB Technical Report, TR-09-34, SKB Stockholm.

Birgersson M., Karnland O., (2009). Ion equilibrium between montmorillonite interlayer space and external solution –consequences for diffusional transport. Geochim. Cosmochim. Acta 73, 1908-1923.

Hedström M., Karnland O., (2012). Donnan equilibrium in Na-montmorillonite from a molecular dynamics perspective. Geochim. Cosmochim. Acta 77, 266-274.

Karnland O., Olsson S., Nilsson U. (2006). Mineralogy and Sealing Properties of Various Bentonites and Smectite-rich Clay Material. SKB Technical Report, TR-06-30, SKB Stockholm.

Schatz T, Kanerva N, Martikainen J, Sane P, Olin M, Seppälä A, Koskinen K, (2013). Buffer erosion in dilute groundwater. POSIVA 2012-44. Posiva Oy, Olkiluoto, Finland.

Results from B+ Tech Oy.

Background

This section of the report summarizes work conducted at B+Tech during the 12 month period from 1.6.2013 to 1.6.2014 of the BELBar Project. The work described below is related to BELBaR deliverable D2.5 “Progress report on erosion processes under flowing water conditions” and covers factors other than water chemistry and clay chemistry (which are described in BELBaR deliverable D2.4 “Progress report on the effects of water chemistry and clay chemistry on erosion processes”) affecting erosion.

The work at B+Tech is conducted mainly using small-scale, flow-through, artificial fracture systems in which swelling clay material can extrude/erode into a well-defined, intersecting fracture (see Figure 1). These experiments are performed in order to simulate the potential extrusion/erosion behavior of bentonite buffer material at a transmissive fracture interface. Using such systems the effect of solution chemistry (salt concentration and composition), material composition (sodium montmorillonite and admixtures with calcium montmorillonite, natural bentonites), flow velocity, fracture geometry (aperture, down-slope) and the role of accessory minerals on erosion processes can be analyzed.

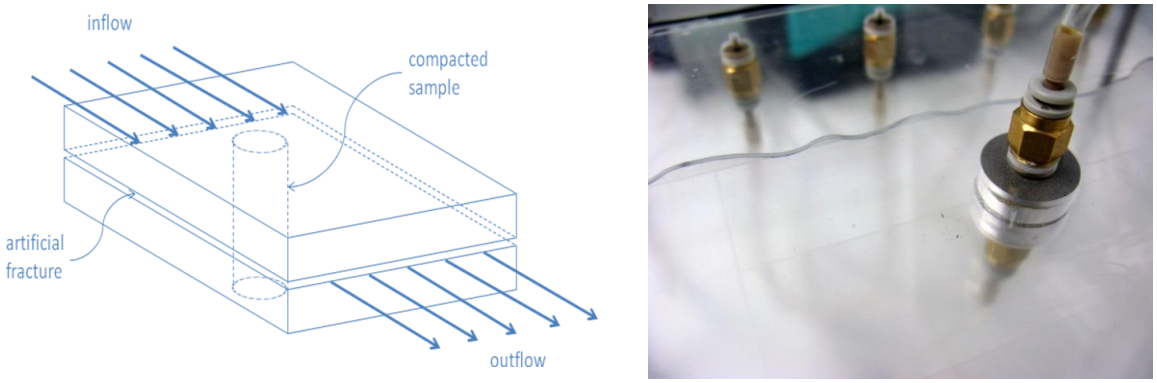

Figure 1. *Schematic representation of the flow-through, artificial fracture test system design basis (left) and photographic image of a flow front approaching a compacted sampled through a 1 mm aperture fracture (right).*

Fate of accessory minerals

As described previously in BELBaR deliverable D2.2, it was observed that accessory phases (kaolin, quartz sand, chromatographic silica) mixed with purified sodium montmorillonite remain behind and form layers near the solid/liquid interface during erosive loss of montmorillonite through contact with dilute groundwater at a transmissive fracture interface.

In order to examine whether the erosion of a more natural bentonite material would result in the observation of similar behaviour, a laboratory test was performed in a flow-through, horizontal, 1 mm aperture, artificial fracture system using MX-80 bentonite washed free of

soluble material and thoroughly exchanged with sodium cations (to ensure the development of erosive conditions). The natural, insoluble accessory minerals remained in the sample material. This material was compacted into a dense sample tablet with a dry density of ~1.6 g/cm^3 and brought into contact with a Grimsel groundwater simulant (relative to Na^+ and Ca^{2+} concentration only) solution at an average flow rate of 0.09 ml/min through the artificial fracture for a period of 865 hours (see Figure 2).

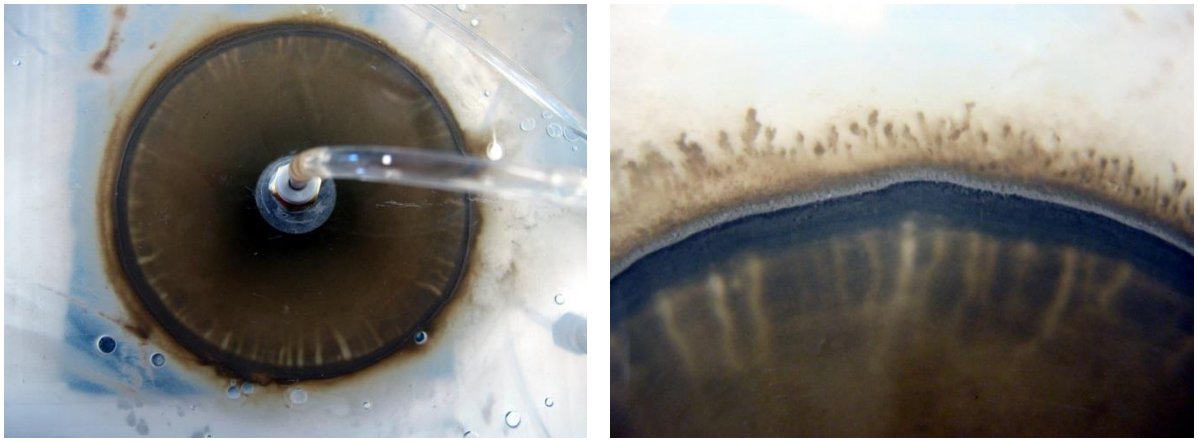

Figure 2. *Photographic images of artificial fracture test with conditioned MX-80 bentonite in contact with Grimsel groundwater simulant at an average flow rate of 0.09 ml/min through a 1 mm aperture frature after approximately 600 h. The grey appearing layer is thought to be composed mainly of accessory phases.*

Once the flow was stopped, the cell was disconnected from the pump and placed into a laboratory oven and dried at 60° C for 48 h and at 105° C for an additional 24 h. After drying was completed the cell was opened and samples were collected at various extrusion distances from the dried material. XRD analyses were performed on the samples followed by full pattern fitting to determine mineralogical compositions. The results are presented in Figure 3.

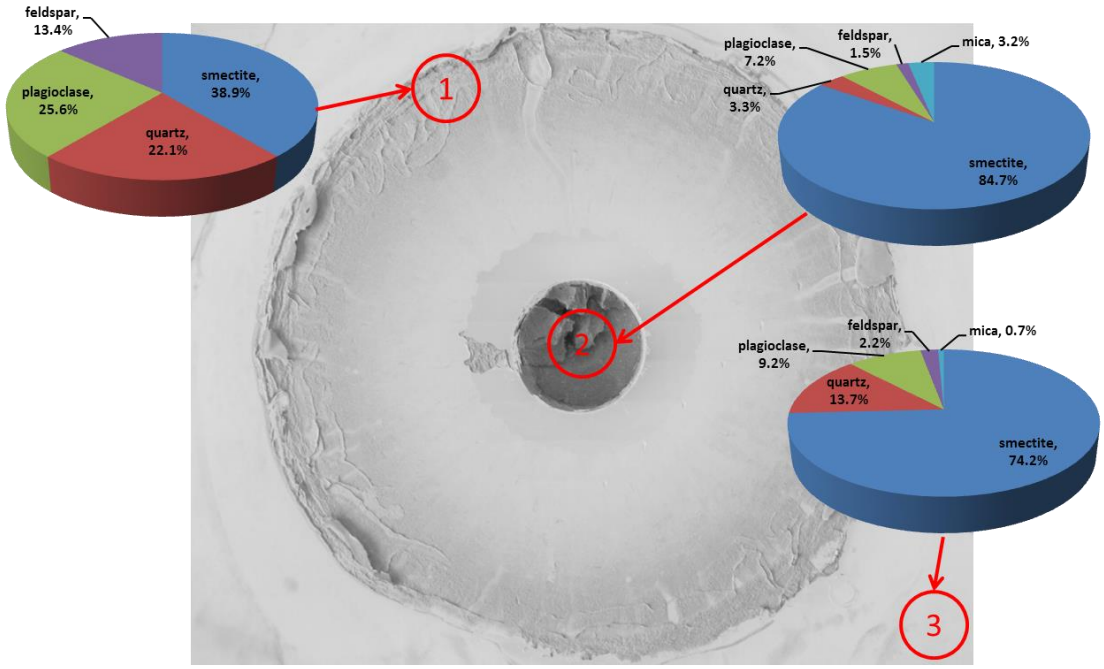

Figure 3. *Photographic image of dried sample from flow-through test in artificial fracture with conditioned MX-80 overlaid with mineralogical composition results from samples at the indicated positions.*

As indicated in Figure 3, the sample material at the erosion interface (sample 1) contains a much larger fraction of accessory phases than the residual sample material (sample 2). This result is consistent with the earlier results showing that added accessory phases remain behind and form layers near the solid/liquid interface during erosive loss of montmorillonite. The mineralogical composition of the residual sample material is essentially identical to that of the starting material. The eroding material (sample 3) is predominantly smectite as well indicating that the clay mineral is the primary eroding phase. The presence of accessory mineral phases in sample 3 does not necessarily indicate that the interfacial accessory mineral layer was unstable to erosion during the test as partial release of these materials may have occurred as a result of tilting during post-mortem fracture transfer. A test using sodium montmorillonite mixed with quartz sand in a 45° sloped fracture (see following section for further information on tests in sloped fractures) showed that both clay and sand were lost from the extruding material.

Effect of fracture slope angle

As discussed in BELBaR deliverable D2.2, a series of artificial fracture tests conducted in fractures positioned at steep slope angles (see Figure 4) for sodium montmorillonite or 50/50 calcium/sodium montmorillonite (all from MX-80 type bentonite) against deionized water or Grimsel groundwater simulant (relative to Na^+ and Ca^{2+} concentration only, i.e., 0.68 and 0.14 mM, respectively) were initiated. Tests were performed using downhill, uphill and stagnant (no) flow conditions.

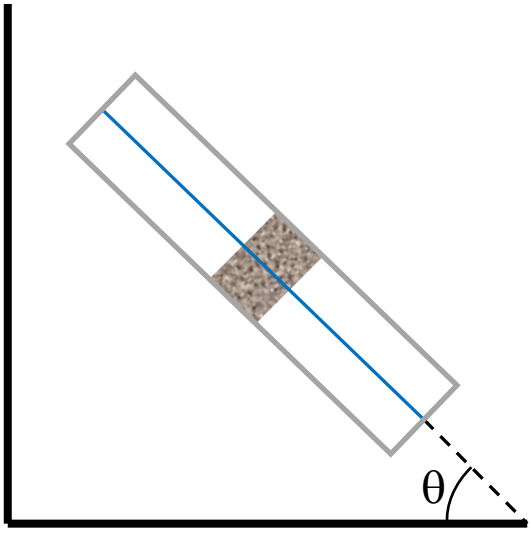

Figure 4. *Schematic diagram showing artificial fracture test system positioned at steep slope angles ($\theta \geq 45°$).*

From a purely visual perspective, clay mass appears to be lost from the extruded source material in artificial fracture tests at steep slope angles via a predominantly sedimentary process (see Figure 5), compared to horizontal fractures where the mass is released by dispersion (see Figure 6). Interestingly, as indicated in Figure 5, the sedimenting bodies are themselves not the same between the 45° case (particulates) and the 90° case (ribbons of gel-like material). It is also the case, as opposed to horizontal fractures, that steady-state extrusion distances are not established in the tests at steep slope angles, i.e., extrusion distances recede with mass loss over time. Moreover, the shape of the extruded zone becomes somewhat egg-shaped with only one axis of symmetry remaining as more mass is lost from the lower half of the extrudate than the top.

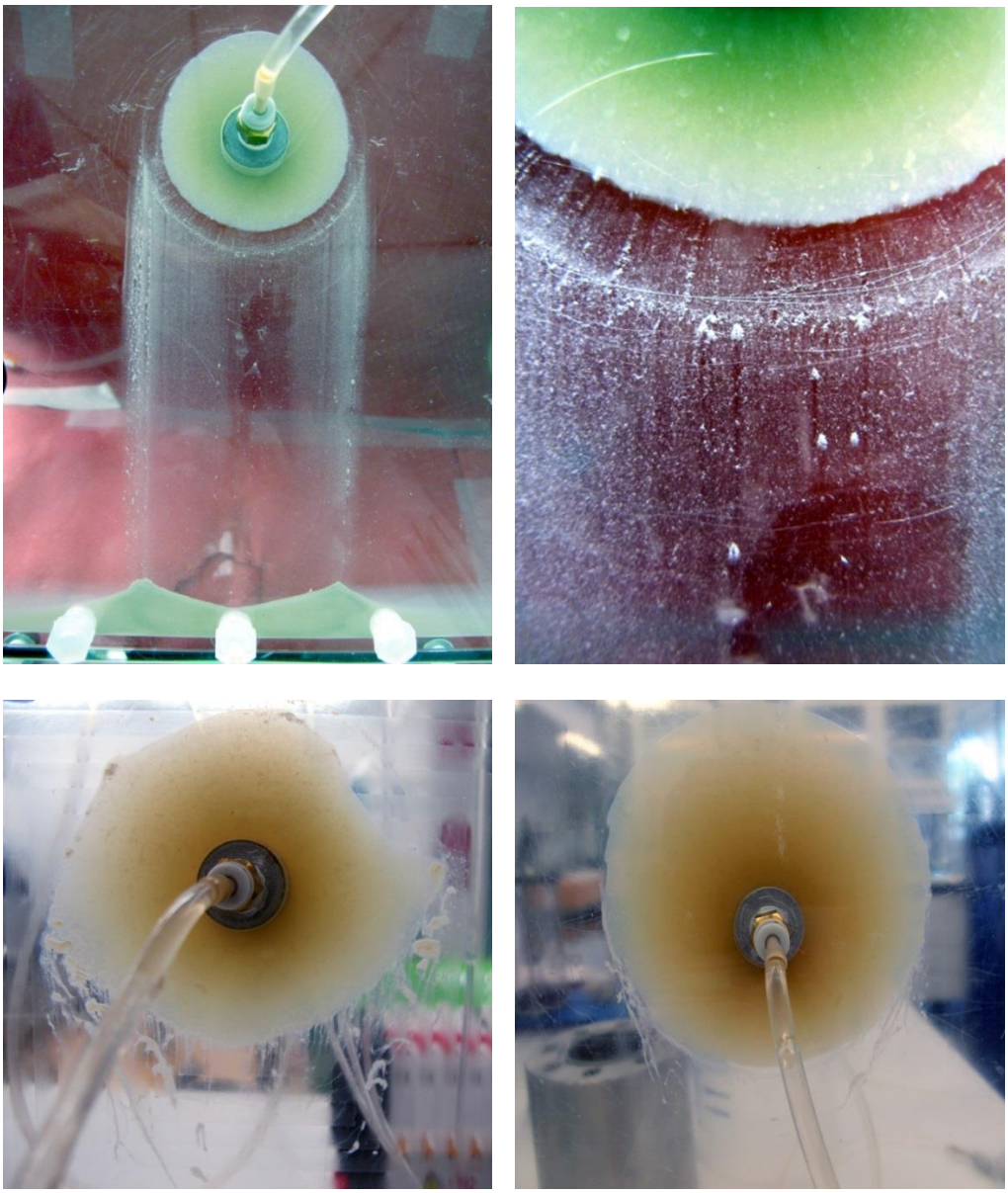

Figure 5. *50/50 calcium/sodium montmorillonite in contact with a Grimsel groundwater simulant at an average flow rate of 0.09 ml/min down a 1 mm aperture artificial fracture system positioned at a 45° slope angle approximately 672 hours after start of test (top images). Sodium montmorillonite in contact with deionized water (bottom left image) and a Grimsel groundwater simulant (bottom right image) at average flow rates of 0.09 ml/min down 1 mm aperture artificial fracture systems positioned at a 90° slope angle approximately 672 hours after start of test.*

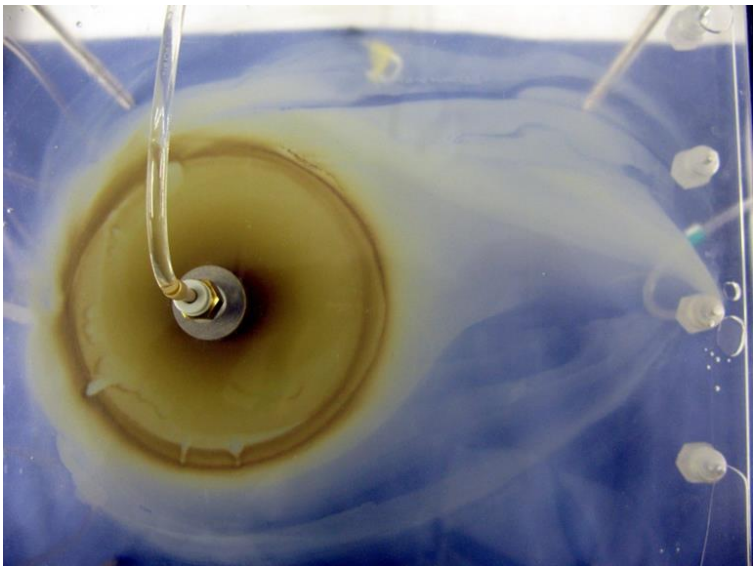

Figure 6. *Sodium montmorillonite in contact with a Grimsel groundwater simulant at an average flow rate of 0.09 ml/min through the 1 mm aperture artificial fracture system positioned horizontally. Image taken 672 hours after start of test.*

In the steep slope angle artificial fracture tests, the sedimenting mass (eroding mass) settles to the bottom of the artificial fracture cells and cannot be fully transported away in the effluent flow through the single outflow port (see Figure 5, top left image). For the purposes of determining mass loss in these tests, material mass other than extant extruded mass or residual emplaced mass at the time the test is stopped is considered to be lost. Average mass loss rates in the sloped fractures were always larger than those of the corresponding horizontal cases. In both the 45° and 90° cases, average mass loss rates were faster by a factor of approximately 1.6 compared to the horizontal cases. The relative equivalence of the average mass loss rates at slope angles of 45° and 90° indicates that whatever additional force is imposed on the extruding material at 90° doesn't lead to significantly more mass loss than what is already achieved at 45°. However, as described above, the sedimenting bodies do not appear to be the same.

Such sedimentary mass loss is also observed in sloped fractures under stagnant (no) flow conditions. In the presence of imposed flow down the sloped fractures, mass loss rates were increased, over the stagnant case, by factors of 3 to 4 with flow velocities from 6.2×10^{-6} to 1.8×10^{-4} m/s.

Insofar as the sedimenting mass could not be effectively carried away in the effluent outflow with its release using the current artificial fracture cell design, an additional series of tests were performed, using a 45° fracture slope angle with sodium montmmorillonite against Grimsel groundwater simulant with an average flow rate of 0.09 ml/min in a 1 mm fracture aperture, to determine mass loss rate as a function of time. The results from these tests (see Figure 7) indicate that a steady-state mass loss rate of 2×10^{-9} kg/s is established after approximately 200 to at least 720 h.

The erosion data described above can be applied to determine bounding estimates of such mass loss due to sloped, saturated fractures intersecting deposition holes (or drifts). Assuming the measured, steady-state erosion rate scales with sample (or deposition hole) diameter, and that the extrusion distance itself behaves and scales similarly, an erosion rate of 5.6 kg/yr is implied (see box 1). Of course the mean fracture aperture in the repository environment may

likely be lower than that in the experiments and it is reasonable to assume that corresponding erosion rates will be smaller as well. Furthermore, explicit relationships between erosion rate and aperture and between erosion rate and sample diameter are yet to be determined. It should also be pointed out that the relative conservativeness of applying results derived from sodium montmorillonite to bentonite behaviour is unknown.

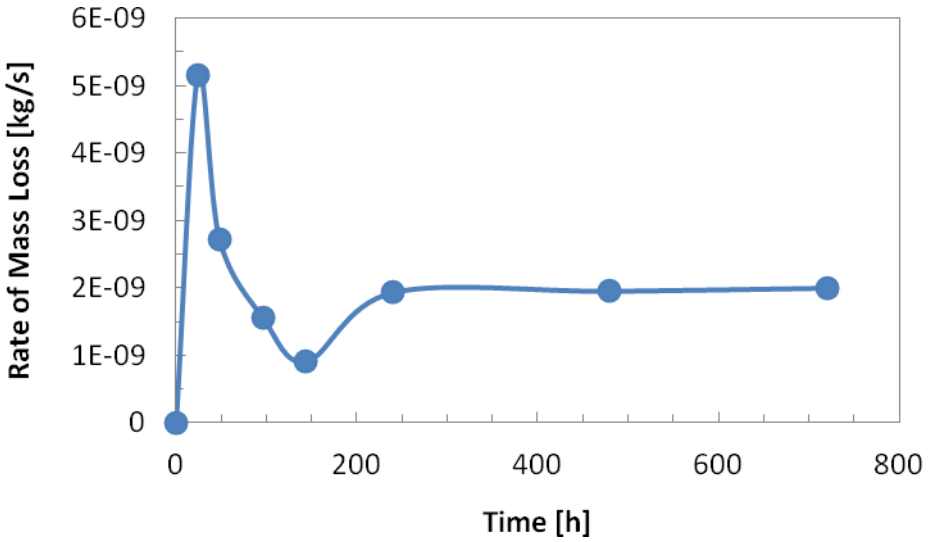

Figure 7. *Average mass loss rates at various test durations for sodium montmorillonite in contact with a Grimsel groundwater simulant at an average flow rate of 0.09 ml/min through a 1 mm aperture artificial fracture system positioned at a 45° slope angle.*

Box 1. Application of Sloped-Fracture Results

- Experimental Dimensions
  radius = 0.01 m (initial sample)
  aperture = 0.001 m (artificial fracture)
  eroding surface area (SA_e) = $2\pi rh = 6.3\times10^{-5}$ m^2

- Unit Erosion Rate (r) [$kg/m^2 \cdot s$]
  E = 2×10^{-9} kg/s (measured, steady-state erosion rate)
  r = $E/SA_e = 3.2\times10^{-5}$ $kg/m^2 \cdot s$

- Repository Dimensions
  radius = 0.875 m (deposition hole)
  aperture = 0.001 m (intersecting fracture)
  eroding surface area (SA_R) = 5.5×10^{-3} m^2

- Upscaled Erosion Rate (E_R)
  $E_R = r \bullet SA_R$ = 1.8×10-7 kg/s = 5.6 kg/y

Effect of surface roughness

In order to examine the effect of surface roughness on the extrusion/erosion behaviour of bentonite buffer material at a transmissive fracture interface, a new rough-walled artificial fracture cell was built which incorporates structured acrylic material (see Figure 8) covering the fracture surfaces. This material has topographical features from the micron to millimeter scale.

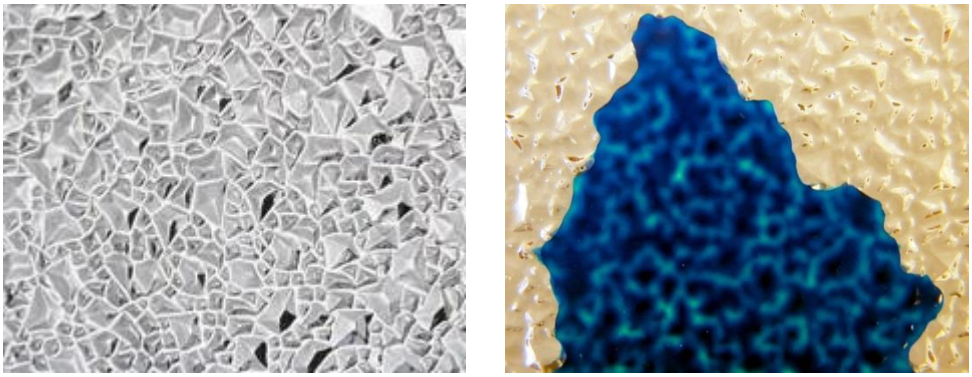

Figure 8. *Images* of *structured acrylic material (left) used to cover the upper and lower fracture surfaces in the rough-walled, artificial fracture system and aliquot of blue dye between two such fracture plates (right). The color intensity distribution of the dye indicates the profile heterogeneity within the fracture and the potential for tortuous flow patterns.*

On the basis of a fracture void volume measurement, the average aperture of the rough-walled, artificial fracture system was evaluated to be 0.95 mm. An intial test (see Figure 9) was conducted in this system using sodium montmorillonite (from MX-80) in contact with deionized water at an average flow rate of 0.09 ml/min for 760 h.

Figure 9. *Photographic image of rough-walled, artificial fracture test with sodium montmorillonite in contact with deionized water after approximately 600 h.*

A comparison of the results from the rough-walled, artificial fracture system to tests run in the smooth-walled, system at 1 mm aperture using the same material, solution and inflow rate

conditions indicates that the average mass loss rate is lower in the rough-walled system by a factor of 2.4. Furthermore, extrusion behaviour differs between the smooth and rough environments in that a steady-state distance is approached in the smooth-walled system but not in the rough-walled system. The rate of extrusion is also lower in the rough-walled system.

Natural fractures are characterized by rough surfaces and complex fluid flows and, as the limited data described here indicates, buffer mass loss in rough-walled fractures may be significantly attenuated relative to that in smooth-walled systems.

Results from erosion experiments performed by ÚJV Řež, a. s.

The conceptual model was described in previous report, deliverable D2.2. The main aim of the erosion experiments is focused on the bentonite in saturation phase, where both the mechanical and chemical erosion is expected. The chemistry of flowing water have dominant impact on erosion process and its extent. Essentially, the stability of clay dispersion is given by the CCC of coagulant (e.g. cations or anionts in groundwater), which is a minimum concentration of coagulant that causes rapid coagulation. Knowing CCCs enable to decide about stability of clay dispersions in a given groundwater or experimental water based solution.

The czech concept of deep geological repository (DGR) considers the granite as a host rock and the hydrochemistry of groundwater from this granitic environment was summarised in previous report (Rukavičková et al., 2009). Three types of groundwater were identified in granitic Bohemian Massif: groundwater – meteoric water in contact with granite (depths 30 – 100 m), mineral groundwater – meteoric water in contact with granite and deep CO_2 and fossil groundwater – old saline waters. The expected chemistry of groundwater in DGR is a combination of these three types. However more groundwater analyses is needed from deeper horizons (300 – 1000 m) to verify the hydrochemistry. The following diagrams shows the main composition of these groundwater (Figure 1).

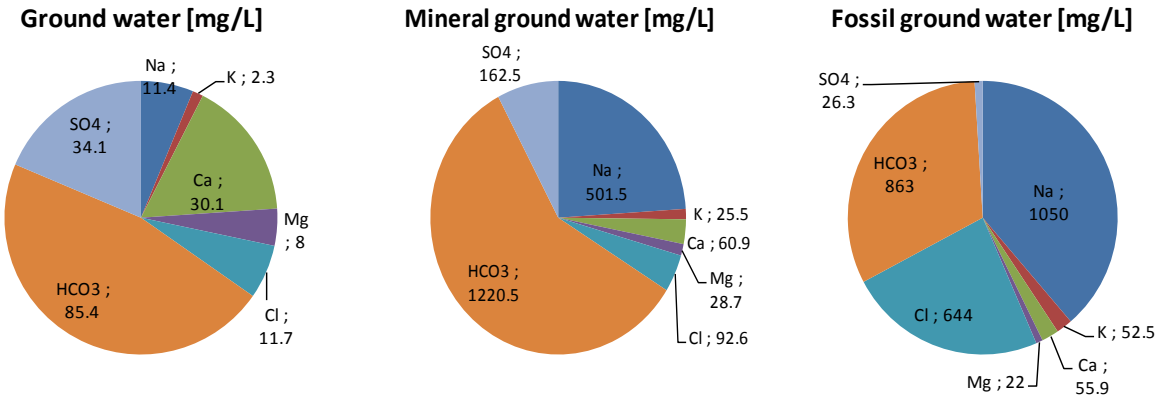

Figure 1.: Main chemistry of three groundwater types from granitic Bohemian Massif (after Rukavičková et al., 2009).

The coagulation experiments, where we study the coagulation of clay dispersions by inorganic cations and anions, suggested, that only for first type of groundwater (meteoric water in contact with granite) the bentonite dispersion should be stable. For other two types of groundwater the bentonite dispersions should coagulated. Because we expected a mixture of these three types of groundwater in the potential granite host rock, the groundwater chemistry is not favourable for long-term stability of bentonite colloids.

Experimental set-up and measurement

The experimental set-up differs from the set-up used by other groups in this project (see Figure 2) and it was described in deliverable D2.2. The main reason for this set-up was to use simple cylindrical arrangement with artificial granite fracture surrounded by compacted bentonite. The flow direction (from bottom to top) was selected mainly for avoiding of air bubbles capture within the apparatus and for homogenous saturation.

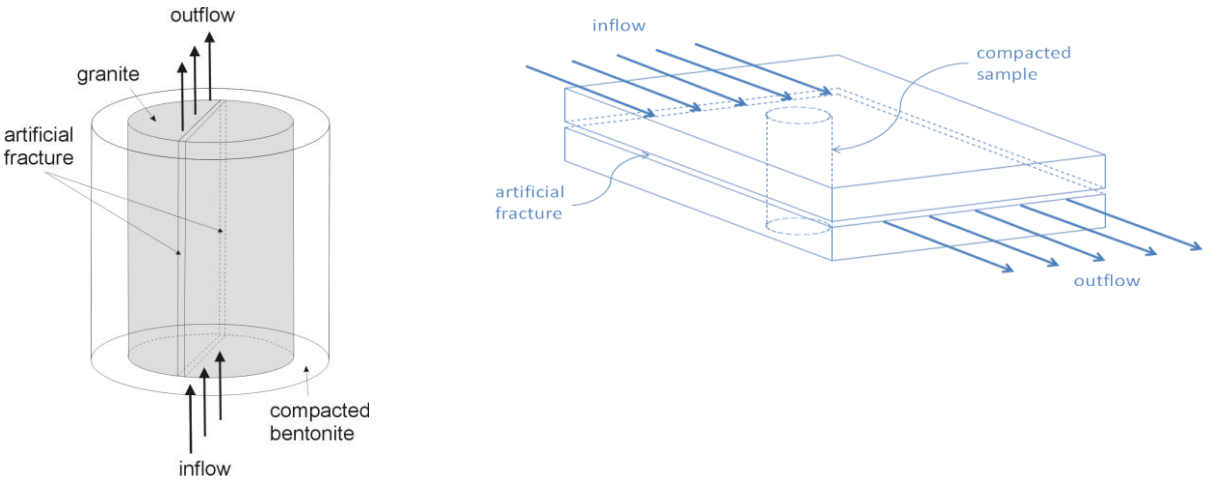

Figure 2.: Experimental set-up with artificial fracture in granite cylinder surrounded by compacted bentonite (ÚJV) – left. Experimental set-up with artificial fracture in between two acrylic blocks and compacted bentonite in the middle – right (Schatz et al., 2013).

Two methods were used for bentonite colloid concentration measurement. First one used Al concentration measured by inductively coupled plasma mass spectrometer (ICP-MS) as a indirect method for clay colloids concentration determination. Because the montmorillonite forms majority in bentonite (60 wt. % for bentonite B75) and therefore the Al content is dominant in comparison with other Al bearing minerals in bentonite, the Al can be used as a indirect tracer for clay colloids. The second method was based on a measurement with photon cross-correlation spectroscopy (PCCS). The calibration curve for estimation of bentonite colloid concentration can be obtained from plotting the response of the photomultiplier (kcps) vs. the known concentration of bentonite colloids (see Figure 3, left). The detection limit for this measurement with PCCS is around 1 mg/L. Comparison of results from both methods showed linear trend, but mainly for higher concentrations (see Figure 3, right). The scatter in low concentrations can be attributed to PCCS detection limit.

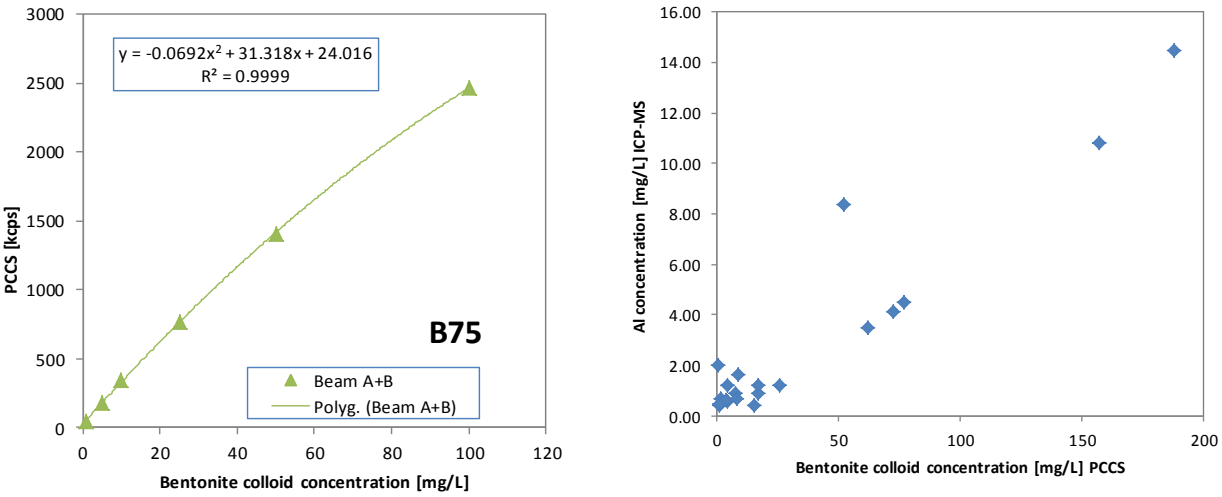

Figure 3.: Calibration curve for measurement of bentonite colloids concentration on PCCS – left. Comparison of both method for measurement of bentonite colloids concentration – right.

Results

The experimental results showed that the erosion rate at a given experimental arrangement reached from 0.4 to 55 kg/m^2/year at flow rates in the range of 5.37×10^{-6} – 2.48×10^{-4} m/s and fracture aperture in the range from 0.15 to 2 mm (Figure 4). The erosion experiments did not show a clear trend between the erosion rate and width of aperture, which is probably caused by the small set of experiments.

All experiments were carried out with distilled water which simulated groundwater with low ionic strength and therefore the extreme conditions with the highest rate of erosion. Mineral separation was observed (probably quartz and biotite) in experiments performed with small fracture aperture from 0.1 to 0.2 mm. This phenomenon may be particularly important mainly for the filtering effect, where the accumulations of small mineral grains can clog pores or fissures and thus prevent the bentonite erosion.

Generally, the chemical-mechanical erosion for Ca-bentonites is less significant than for Na-bentonites. However, it is necessary to consider the ion exchange between groundwater and bentonite, which can result in complete exchange of cations, and thus the selection of Ca- or Na-bentonite may not be the crucial issue.

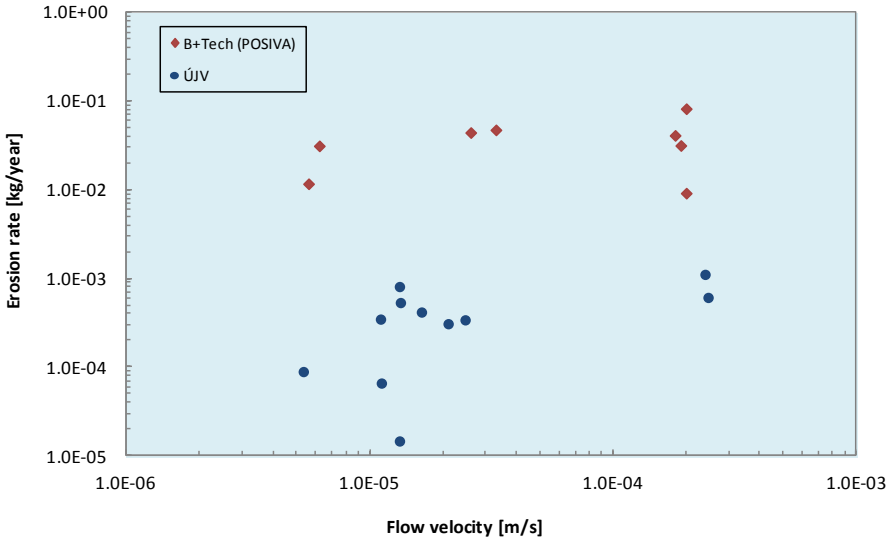

Figure 4.: Comparison of results: Erosion rate vs. flow velocity in log-log scale, blue points ÚJV results, red points POSIVA 2012-44 (Schatz et al., 2013). It has to be noted, that both sets of experiments are mainly differ in the fracture aperture (ÚJV fracture varies from 1.5×10^{-4} to 2.0×10^{-3} and B+Tech used just one size of fracture 1.0×10^{-3}) and liquid phase (ÚJV used only deionized water and B+Tech also NaCl electrolyte in some experiments). Also significant is the flow direction (see Figure 2).

References

Rukavičková L., Pačes T., Holeček J. (2009): Expertní odhad hydraulických a hydrochemických parametrů, DZZ 3.3 projektu „Výzkum procesů pole vzdálených interakcí HÚ vyhořelého jaderného paliva a vysoce aktivních odpadů“. ČGS Praha, 77 str.

Schatz T, Kanerva N, Martikainen J, Sane P, Olin M, Seppälä A, Koskinen K, 2013. Buffer erosion in dilute groundwater. POSIVA 2012-44. Posiva Oy, Olkiluoto, Finland.

Report of the work performed at KIT-CN/INE

Summary

At KIT-CN/INE the erosion and swelling behavior of the FEBEX bentonite has been investigated. Therefore erosion experiments were conducted in custom-made flow through cells. During the experiments the bentonite swelling pressure was monitored and the colloid concentration and the colloidal size distribution were measured. In this report preliminary results of these measurements are presented.

Set-ups for erosion experiments

At KIT-CN/INE the erosion and swelling behaviour of the FEBEX bentonite has been investigated during erosion experiments conducted in a custom-made flow through cell. Figure 1 shows the set-up of these kinds of cells. The housing is made of acrylic glass and has a diameter of 18 cm and an aperture of 1 mm. For the tests compacted FEBEX bentonite rings (inner diameter: 4 cm, outer diameter 8 cm, height: 2.5 cm) were used, which were provided by CIEMAT (initial density: 1650 kg/m^3). The rings were placed in a cavity in the center of the cell and were dry prior to the experiment. Grimsel groundwater was pumped through the cell by a peristaltic pump with an initial flow velocity $v_{init.} = 10^{-5}$ m/s.

Mineralogical characterization of the erosion-"halo"

One of the two setups was used to observe the evolution of the "halo"-like structure of eroded material which was formed within the 1 mm aperture (Figure 1a). After 40 days the erosion halo did not expand anymore (final diameter of 2-2.5 cm) and the experiment was stopped. Details about the sampling procedure and the results of the mineralogical characterization are presented in Deliverable 2.6.

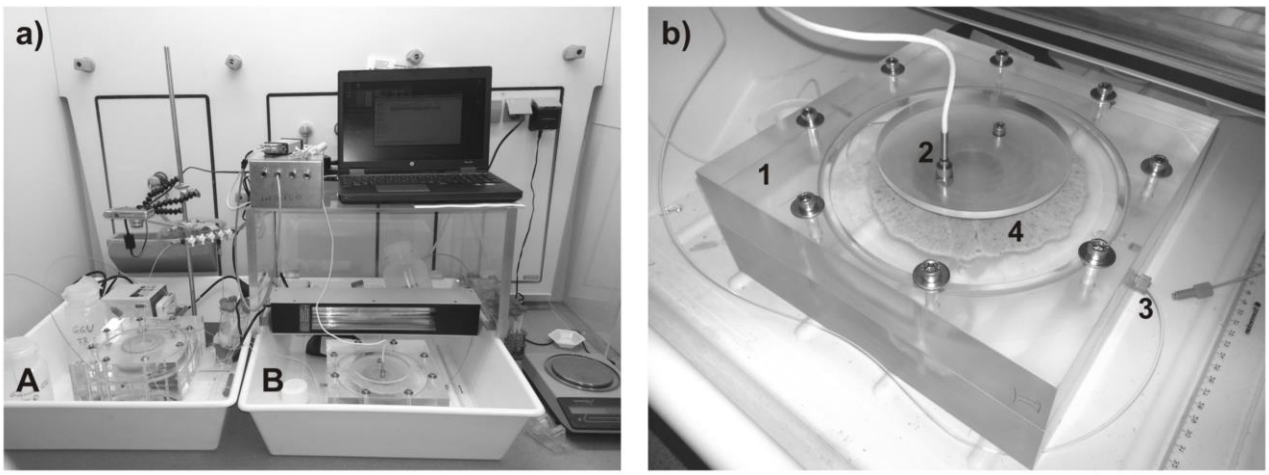

Figure 1. a) setup of the erosion experiments. Setup (A) on the left with the experiment for the mineralogical characterization of the erosion-"halo". Setup (B) on the right: long-term erosion experiment equipped with a pressure sensor. b) Setup (B) during the experiment, visible are the acrylic glass housing (1), the pressure sensor (2) with the (dark) bentonite ring beneath, the water inlet (3) and the erosion halo (4).

The second setup is used for a long-term experiment (Figure 1b). It is running continuously since October 2013. Here the bentonite ring was filled with eight thin glass vials containing

220 mg (synthetic Ni-labelled) montmorillonite (as paste), spiked with 10 mg uranine in each vial as conservative tracer and the homologues Eu, Th, Hf and Tb (25 µg per vial, respectively). Therefore, eight holes were drilled laterally to mount the glass vials. Due to the swelling of the clay the glass vials are supposed to break and release the labelled montmorillonite and associated tracers as well as the conservative tracer. Furthermore this cell was equipped with a pressure sensor (disynet XP1103-A1-100BG) to monitor the evolution of the bentonite swelling pressure during the experiment (Figure 1, b.2).

Measurement of swelling pressure

Within the first 24 h after the start of the experiment the swelling pressure rises up to 2.6 MPa (Figure 2a). During the following days the pressure decreases to a constant value between 1.7 to 1.8 MPa implying steady state conditions (Figure 2b). This pressure drop coincides with the bentonite swelling into the 1 mm aperture.

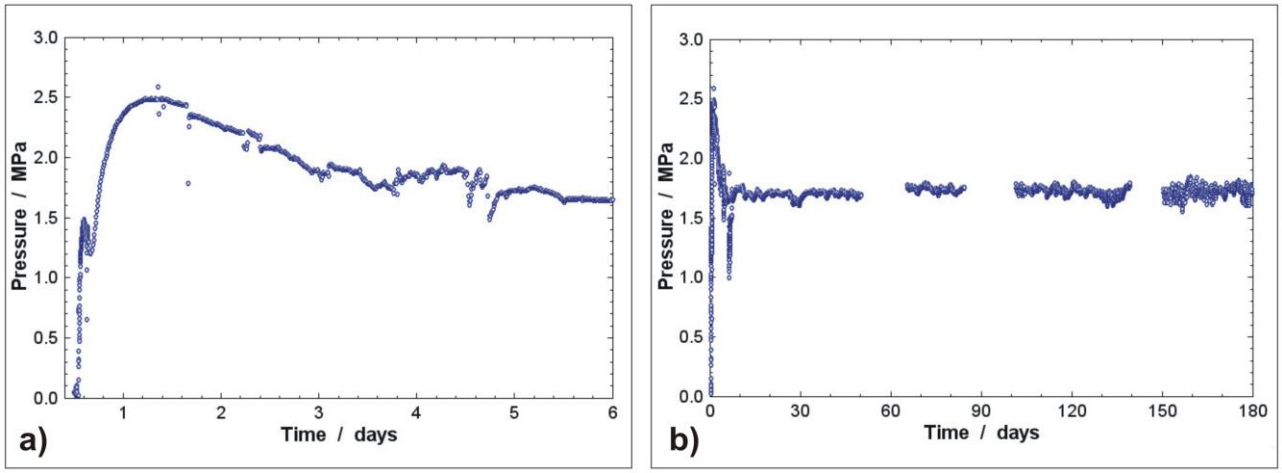

Figure 2. Results of pressure measurements over a time period of 180 days.

Water samples of the reactor effluent are taken daily for analysis of elemental composition, fluorescence, pH, colloid size and concentration. These data are evaluated within the following months. The colloidal size distribution and concentration obtained is depicted in Figure 3.

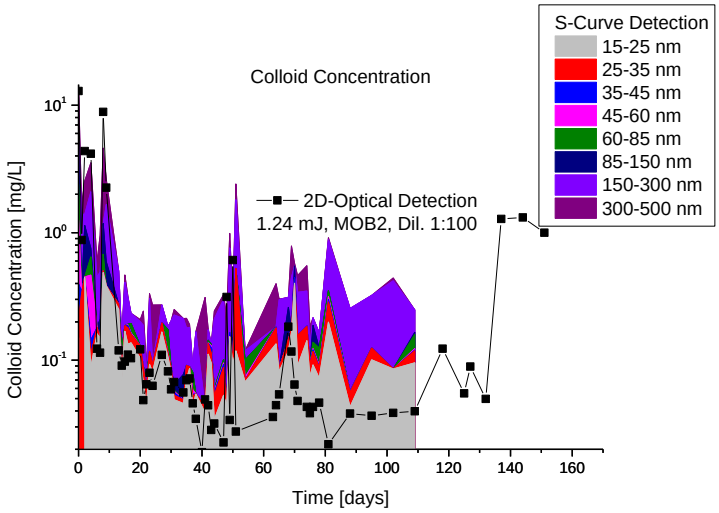

Figure 3. Colloidal size distribution measured by s-curve LIBD and MOB2-LIBD.

During the first days of the experiment a high colloid concentration is detected (initially ~10 mg/l) which could be explained by the release of most likely accessory minerals and loosely aggregates during the initial saturation of the setup followed by a decrease of colloid concentration to values around 0.2 to 1 mg/l after 50 d. The results obtained so far are in line with previous performed experiments. In the previous experiments the colloid concentration increased to 10 mg/l reaching equilibrium conditions after 100 d.

Colloid separation by centrifugation

To prepare colloids by centrifugation and in order to achieve a colloid size range and composition that is as similar as possible to the colloids formed by the bentonite erosion tests, one of the bentonite rings was pulverized and sieved until an uniform grain size below 63 µm was reached. The material was dispersed in de-ionized water (< 16.2 µS/cm) (1 wt.-% bentonite) for one day to remove soluble phases. During the first three washing steps the supernatant was removed by centrifugation (2.8 g, 30 min). A further centrifugation was not possible under these conditions, due to decreasing ionic strength and therefore increasing colloid stability. Dialysis until conductivity was below 5 µS/cm completed the washing procedure.

Centrifugation at 2.8 g was used to separate the colloidal phase from the larger particle fractions. A test showed that centrifuging for 10 minutes yields best results. The size distribution and concentration of the colloidal dispersion was determined by LIBD, S-curve LIBD and ICP-OES. In the case of ICP-OES measurements the colloid concentration was determined by the structural formula of the bentonite for the results of Mg^{2+}, Al^{3+} and Fe^{3+} and the mean value of these elements is formed. The results are given in Table 1.

Table 1. Colloid concentration and average diameters.

Centrifugation time [min]	$C_{ICP-OES}$ [g/L]	C_{LIBD} [g/L]	D_{LIBD} [nm]	C_{s-LIBD} [g/L]
5	1.57	2.37	125	1.66
10	0.87	1.19	118	1.54
30	0.36	0.70	91	0.70